



Photoelectron spectroscopy and density functional theory study of Bi_2Al_n^- ($n = 1\text{--}4$) clusters



Zhang Sun^a, Hong-Guang Xu^{b,*}, Gang Feng^b, Xi-Ling Xu^b, Wei-Jun Zheng^b

^a College of Chemical Engineering, Hebei United University, Tangshan 063009, PR China

^b Beijing National Laboratory for Molecular Sciences (BNLMS), State Key Laboratory of Molecular Reaction Dynamics, Institute of Chemistry, Chinese Academy of Sciences, Beijing 100190, PR China

ARTICLE INFO

Article history:

Received 20 June 2014

In final form 18 September 2014

Available online 6 October 2014

ABSTRACT

The Bi_2Al_n^- ($n = 1\text{--}4$) clusters were investigated by anion photoelectron spectroscopy and density functional theory calculations. By photoelectron spectroscopy the vertical detachment energies of Bi_2Al_n^- ($n = 1\text{--}4$) were determined to be 2.12 ± 0.08 , 2.32 ± 0.08 , 2.66 ± 0.08 , and 2.15 ± 0.08 eV, respectively. The structures of Bi_2Al_n^- ($n = 1\text{--}4$) were determined by comparison of photoelectron experiments and calculations. It is found that Bi_2Al_n^- ($n = 1\text{--}4$) anions all have a Bi_2 unit inside their structures, in which the Bi–Bi bond lengths are in the range of 2.81–3.08 Å. The natural population analysis shows that the negative charges mainly localized on the Bi_2 unit inside the most probable structures.

© 2014 Elsevier B.V. All rights reserved.

1. Introduction

The alloys of III–V elements are important materials in the fabrication of fast microelectronic devices and light-emitting diodes [1], and also these alloys, such as Bi/Al alloys, have important metallurgical characteristics [2] and electrochemical behavior [3]. The detailed study on the structural and electronic properties of the clusters of III–V elements as a function of their sizes may provide insight into the evolution of the properties of alloys from molecular level to the bulk.

In the last decades, the clusters consisting of III–V elements were investigated intensively by experiments [4–10] and theoretical calculations [11–17]. Neumark and co-workers [4–6] studied the size selected Al/P, Ga/P, In/P, and Ga/As cluster anions by photoelectron spectroscopy (PES). Kamal et al. investigated Ga_nP_n ($n = 2\text{--}5$) clusters using density functional theory (DFT) calculations [16]. Bel-Bruno studied the electronic and geometric structures as well as the bonding properties of small Ga_nAs_m clusters by DFT calculations [12]. Guo [14] reported the theoretical studies of the Al_mAs_n cluster anions. Quek et al. [17] reported the tight binding molecular dynamics investigation of Ga_mAs_n and Al_mAs_n clusters. There are also a number of studies on Bi/Al clusters. Li et al. [18] studied the mechanisms of H_2 generation catalyzed by Al_{16}Bi clusters in water and showed that Al_{16}Bi cluster can make fast H_2 generation

rate, high H_2 yields and lasting long-term H_2 production process. Jones et al. [19] reported a study of Bi-doped aluminum clusters, Al_nBi^- ($n = 1\text{--}5$), using photoelectron spectroscopy and DFT calculations. They suggested that Al_3Bi is an all-metal aromatic cluster, and Al_5Bi is a jellium superatom candidate. Sun et al. [10] also studied the Al_mBi_n^- ($m + n \leq 7$) anionic clusters by mass spectrometry and DFT calculations, and suggested that the Al_2Bi_3^- cluster is a gas phase Zintl ion with a stable trigonal bipyramidal structure.

In order to further explore the properties of small-sized Bi/Al clusters, in the present work, we performed a combined PES and DFT study on double Bi atoms doped aluminum clusters Bi_2Al_n^- ($n = 1\text{--}4$) and identified these clusters all have a Bi_2 unit inside their structures. In addition, it is found that the negative charges mainly localized on the Bi_2 unit inside the most probable structures.

2. Experimental and theoretical methods

2.1. Experimental method

The experiments were conducted on a home-built apparatus consisting of a time-of-flight mass spectrometer and a magnetic-bottle photoelectron spectrometer, which has been described elsewhere [20]. Briefly, Bi/Al cluster anions were generated in a laser vaporization source by laser ablation of a rotating disk target (13-mm diameter, Bi/Al atom ratio 1:1) with the second harmonic of a nanosecond Nd:YAG laser (Continuum Surelite II-10). The typical laser power used in this work was ~10 mJ/pulse. Helium with ~4 atm backing pressure was injected by a pulsed

* Corresponding author.

E-mail address: xuhong@iccas.ac.cn (H.-G. Xu).

Table 1

Relative energies and theoretical VDEs and ADEs of the low-lying isomers of Bi_2Al_n^- ($n=1-4$) as well as the experimental VDEs and ADEs estimated from their photoelectron spectra.

	Isomer	State	Point group	ΔE^a	VDE		ADE	
				(eV)	(eV)	(eV)	Cal.	Exp. ^b
				Cal.	Exp. ^b	Cal.	Exp. ^b	
Bi_2Al^-	1a	$^1\text{A}_1$	C_{2v}	0.00	2.18	2.12	2.03	1.94
	1b	$^3\Sigma_g$	$D_{\infty h}$	0.30	2.45		2.43	
Bi_2Al_2^-	2a	$^2\text{A}_1$	C_{2v}	0.00	2.24	2.32	2.18	2.11
	2b	$^2\text{B}_1$	C_{2v}	0.52	2.62		1.66	
	2c	$^2\text{A}_2$	C_{2v}	0.55	2.81		1.63	
Bi_2Al_3^-	3a	$^1\text{A}_1$	C_{2v}	0.00	2.99	2.66	2.66	2.30
	3b	$^1\text{A}_1'$	D_{3h}	0.30	2.67		2.36	
	3c	^1A	C_1	0.45	2.69		2.21	
Bi_2Al_4^-	4a	$^2\text{A}_1$	C_{2v}	0.00	2.23	2.15	2.05	1.84
	4b	$^2\text{B}_1$	C_{2v}	0.37	2.55		1.68	

^a ΔE is the difference of isomer energy relative to the correspondingly lowest lying structure.

^b The uncertainty for the experimental VDE and ADE is ± 0.08 eV.

valve into the source to cool the formed clusters. The generated cluster anions were mass-analyzed with the time-of-flight mass spectrometer. The Bi_2Al_n^- ($n=1-4$) clusters were each selected with a mass gate, decelerated by a momentum decelerator before being photodetached by the laser beam from another Nd:YAG laser (Continuum Surelite II-10, 266 nm). The electrons from the photodetachment were energy-analyzed by the magnetic-bottle photoelectron spectrometer. The photoelectron spectra were calibrated with the spectra of Cu^- and Au^- taken at similar conditions. The resolution of the magnetic-bottle photoelectron spectrometer was ~ 40 meV at electron kinetic energy of ~ 1 eV.

2.2. Theoretical method

The structural optimizations and frequency calculations were carried out using the density functional theory (DFT) with the Becke's three-parameter and Lee–Yang–Parr's gradient-corrected correlation hybrid functional (B3LYP) [21,22]. The 6-311++g (3df) basis set was used for the Al atoms. For the Bi atoms, the LANL2DZ basis set [23] was used, in which the relativistic effective core potentials (RECPs) were incorporated. It has been shown that RECPs are common and efficient ways to reduce the complex calculations for molecules containing heavy atoms such as Bi [9,10,24–26]. The geometry optimizations were conducted without any symmetry constraint. Harmonic vibrational frequencies were calculated to make sure that the structures correspond to the real local minima. Many different spin states were considered for all stable structures. It is found that the most stable structures of cluster anions are all in the lowest spin electronic states (singlet or doublet). All the calculations were carried out with the GAUSSIAN 03 program package [27]. The natural population analysis (NPA) of Bi_2Al_n^- ($n=1-4$) clusters was conducted with the nature bond orbital (NBO) version 3.1 program [28–30] implemented in the GAUSSIAN 09 package [31].

3. Photoelectron spectra of Bi_2Al_n^- ($n=0-4$)

The photoelectron spectra of Bi_2Al_n^- ($n=0-4$) clusters recorded with 266 nm (4.661 eV) photons are shown in Figure 1. By each spectrum the vertical detachment energy (VDE) and adiabatic detachment energy (ADE) of the corresponding cluster were measured and listed in Table 1. The peaks in the spectrum represent the electronic transitions from the anion ground state to the ground state and higher excited states of the neutral species. For the first peak of the spectrum, the value of the maximum intensity is taken as VDE compared with the theoretical VDE. The ADE was determined by drawing a straight line along the leading edge of the first

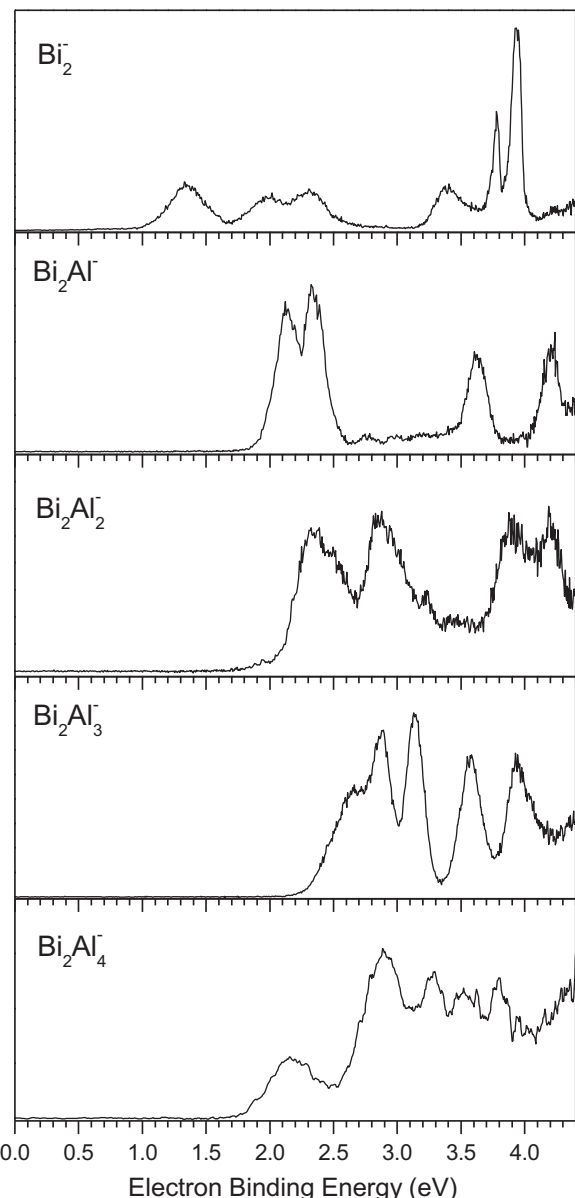


Figure 1. Photoelectron spectra of Bi_2Al_n^- ($n=0-4$) clusters recorded with 266 nm photons.

peak to cross the baseline of the spectrum and then adding the instrument resolution to the electron binding energy (EBE) value at the crossing point.

Bi_2^- has four broad features centered at 1.33, 1.99, 2.31 and 3.40 eV, and two sharp peaks centered at 3.78 and 3.93 eV. The VDE and ADE of Bi_2^- obtained from 266 nm photoelectron spectrum shown in Figure 1 are in agreement with the previous studies [32,33], and the distribution of the current spectrum also agrees well with the previous study reported by Gasusa [32].

As shown in Figure 1, the photoelectron spectrum of Bi_2Al^- is dominated by two intense peaks at 2.12 and 2.33 eV, and two slightly weaker peaks at 3.61 and 4.21 eV. In the spectrum of Bi_2Al_2^- , there are four major broad features centered at 2.32, 2.84, 3.88 and 4.19 eV, and some unresolved peaks between the first and second features. The spectrum of Bi_2Al_3^- shows four resolved features centered at 2.88, 3.14, 3.57 and 3.92 eV, and a shoulder before the first peak in the range of 2.27–2.76 eV. It will be shown later that the spectrum of Bi_2Al_3^- is contributed by different isomers. In

the case of Bi_2Al_4^- , the spectrum shows five barely resolved peaks centered at 2.15, 2.89, 3.28, 3.52 and 3.81 eV, respectively.

From the above, the Bi_2Al_3^- cluster shows larger VDE and ADE than the other clusters. This is because that the Bi_2Al_3^- cluster has a closed shell electronic structure. The electrons in a doubly occupied HOMO will feel a stronger effective core potential due to less effect of the electron screening for electrons in the same orbital than for the inner shell electrons. It needs more energy to remove an electron in the doubly occupied HOMO. This idea will also be presented further by the following molecular orbital analysis.

4. Theoretical results and discussion

The optimized geometries of the low-lying isomers of the Bi_2Al_n^- and Bi_2Al_n ($n=1-4$) clusters are presented in Figures 2 and 3, respectively. The Cartesian coordinates of the low-lying isomers of the Bi_2Al_n^- and Bi_2Al_n ($n=1-4$) clusters are available in the supplementary material. The relative energies between these isomers as well as their theoretical VDEs and ADEs are also summarized in Table 1. It can be seen from Figure 2 that two Bi atoms tend to form Bi–Bi bond in the most stable structures of Bi_2Al_n^- ($n=1-4$) clusters. The Bi–Bi bond length in Bi_2Al_n^- cluster is 2.81 Å, close to that of Bi_2^- dimer (2.77 Å) [34], which shows that the more Al atom has little effect on the $\pi-\pi$ bond of the Bi_2^- dimer. The Bi–Bi bond length in Bi_2Al_n^- ($n=2-4$) clusters is about 3.00 Å, in agreement with the average bond length of anionic Bi_n^- clusters [35]. It shows that the increase of Al atom number results in the increase of the Bi–Bi bond length in the Bi_2^- dimer. This idea will also be discussed further by following the molecular orbital analysis.

We have also simulated the photoelectron spectrum of each isomer based on theoretically generalized Koopmans' theorem [36,37], in which each transition corresponds to removal of an electron from a specific molecular orbital of the anionic cluster. In the simulation, we first set the transition related to the highest occupied molecular orbital (HOMO) of the anionic cluster to the position of VDE, and shifted the transitions of the deeper orbitals according to the HOMO transition. For convenience, we call the simulated spectrum as density of states (DOS) spectrum [37], and the energy levels are plotted as sticks in the DOS spectra. The simulated DOS spectra and experimental spectra of Bi_2Al_n^- ($n=1-4$) clusters are compared in Figure 4. It can be seen that the theoretical simulated DOS spectra of the most stable isomers of Bi_2Al_n^- fit the experimental spectra quite well. Furthermore, we also analyzed the orbital compositions of the most possible anionic clusters and the

calculated molecular orbital (MO) pictures for Bi_2Al_n^- ($n=1-4$) clusters are given in Figure 5.

4.1. Bi_2Al^-

As shown in Figure 2, the most stable isomer (1a) of Bi_2Al^- cluster is a triangular structure with C_{2v} ($^1\text{A}_1$) symmetry, and the linear isomer (1b) with $D_{\infty h}$ ($^3\text{S}_g$) symmetry is 0.30 eV higher in energy than isomer 1a. The calculated VDE of isomer 1a is 2.18 eV, which is in agreement with the experimental value of 2.12 eV. The VDE of isomer 1b is 2.45 eV, much higher than the experimental value.

The simulated DOS spectrum of isomer 1a agrees well with the experimental PE spectrum of Bi_2Al^- cluster. On the other hand, the simulated spectrum of isomer 1b is not in agreement with the experimental PE spectrum. Therefore, isomer 1a is the most likely structure for Bi_2Al^- cluster.

We also analyzed the molecular orbital (MO) pictures of isomer 1a (as shown in Figure 5). We can see that HOMO-2 is the big π bond in the Al–Bi–Bi triangular structure. It needs more energy to pump one electron from HOMO-2 to HOMO-1. Thus, there is a big gap (1.28 eV) between the second and third peaks in the PE spectrum of Bi_2Al^- cluster. Due to the big π bond, the Bi–Bi bond length in the Bi_2Al^- cluster is much smaller than that of other clusters. The Bi–Bi bond length in Bi_2Al^- cluster (2.81 Å) is close to that of Bi_2^- dimer (2.77 Å) [34].

4.2. Bi_2Al_2^-

The most stable structure of Bi_2Al_2^- cluster (2a) is a butterfly structure with C_{2v} ($^2\text{A}_1$) symmetry. Isomers 2b and 2c are 0.52 eV and 0.55 eV higher in energy than isomer 2a, respectively. The calculated VDE of isomer 2a is 2.24 eV, close to the experimental value (2.32 eV). The VDEs of isomers 2b and 2c are 2.62 and 2.81 respectively, much higher than the experimental value.

The simulated DOS spectrum of isomer 2a is in agreement with the experimental PE spectrum of Bi_2Al_2^- cluster. And the simulated spectrum of isomer 2b is not in agreement with the experimental PE spectrum. Thus, we suggest isomer 2a to be the most probable structure of Bi_2Al_2^- .

4.3. Bi_2Al_3^-

For the Al_2Bi_3^- cluster, the most stable structure is isomer 1a with C_{2v} symmetry, in which an Al atom caps on the butterfly

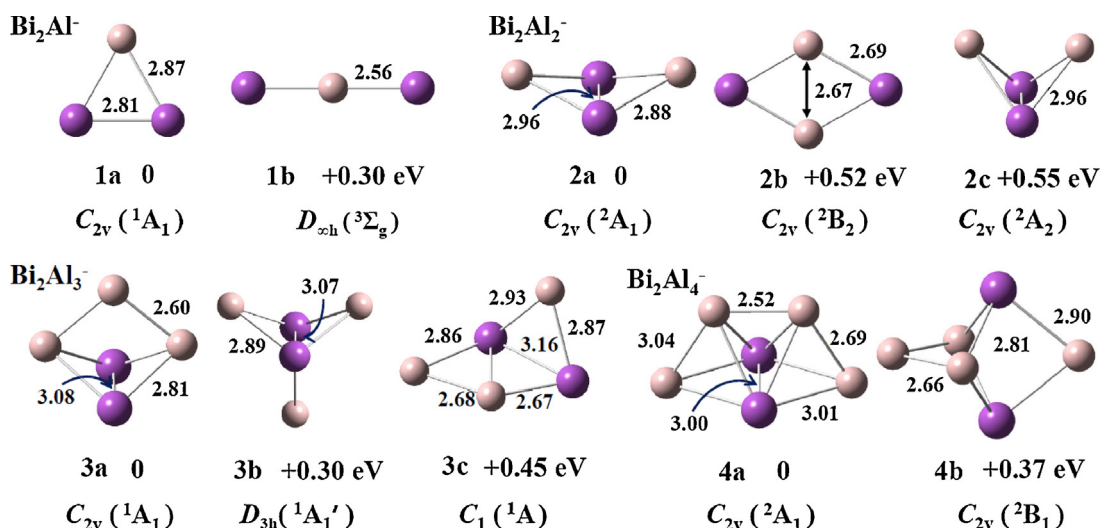


Figure 2. Optimized geometries of the low-lying isomers of the Bi_2Al_n^- ($n=1-4$) clusters. Bond lengths are given in Angstroms, and the relative energies to the most stable isomers are shown.

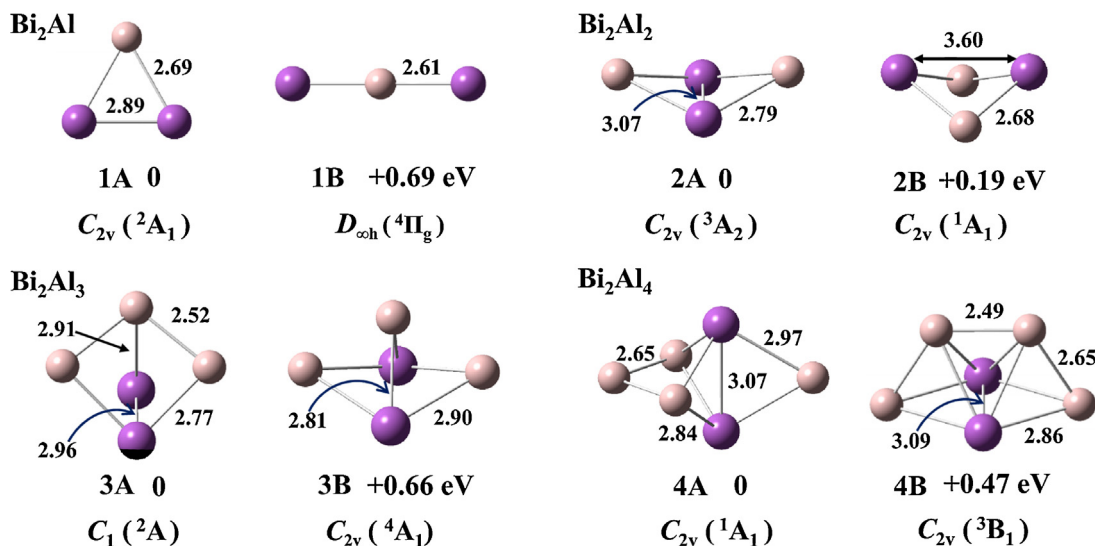


Figure 3. Optimized geometries of the low-lying isomers of the neutral Bi_2Al_n ($n = 1\text{--}4$) clusters. Bond lengths are given in Angstroms, and the relative energies to the most stable isomers are shown.

structure of Bi_2Al_2^- cluster (isomer 2a). Isomer 3b is a distorted bipyramid structure with D_{3h} ($^1\text{A}_1'$) symmetry, which is 0.30 eV higher in energy than isomer 3a. Isomer 3c is 0.45 eV higher in energy than isomer 3a. The calculated VDE of isomer 3a is 2.99 eV, which is higher than the experimental value of 2.66 eV. The VDE of isomer 3b is 2.67 eV, close to the experimental value (2.66 eV). The VDE of isomer 3c is also close to the experimental value, but it is unlikely to be presented in the experiments because it is much less stable than isomer 3a and 3b.

The comparison of the experimental PE spectrum of Bi_2Al_3^- with the simulated DOS spectra of isomers 3a and 3b is shown in Figure 4. The two peaks of the simulated DOS spectrum of isomer 3a are corresponding to the second and fourth peaks in the experimental PE spectrum. While the three peaks remaining in the simulated spectrum of isomer 3b are corresponding to the first, third and fifth peaks in the experimental PE. The simulated DOS spectrum of isomer 3c is not in agreement with the experimental PE spectrum (see the supporting information). Thus, we

suggest that both isomers 3a and 3b contribute to the experimental spectrum.

The Bi_2Al_3^- cluster shows larger VDE and ADE than the other clusters, for the Bi_2Al_3^- cluster has a closed shell electronic structure. The MO pictures for isomers 3a and 3b are given in Figure 5. We can see that HOMO of isomer 3a has a big π bond in the three Al atoms part, and HOMO-1 of isomer 3b has a big π bond in the Al–Bi–Bi part. HOMO of isomer 3a and HOMO-1 of isomer 3b correspond to the second and third peaks in the PE spectrum of Al_2Bi_3^- cluster, respectively. The first peak comes from the HOMO of isomer 3b.

4.4. Bi_2Al_4^-

The most stable structure of the Bi_2Al_4^- cluster is an edge-capped trigonal bipyramidal (4a) with C_{2v} ($^2\text{A}_1$) symmetry, which is built by capping an Al atom on isomer 3a. Isomer 4b with C_{2v} ($^2\text{B}_1$) symmetry is 0.37 eV higher in energy than isomer 4a. The calculated VDE of isomer 4a is 2.23 eV, close to the experimental value

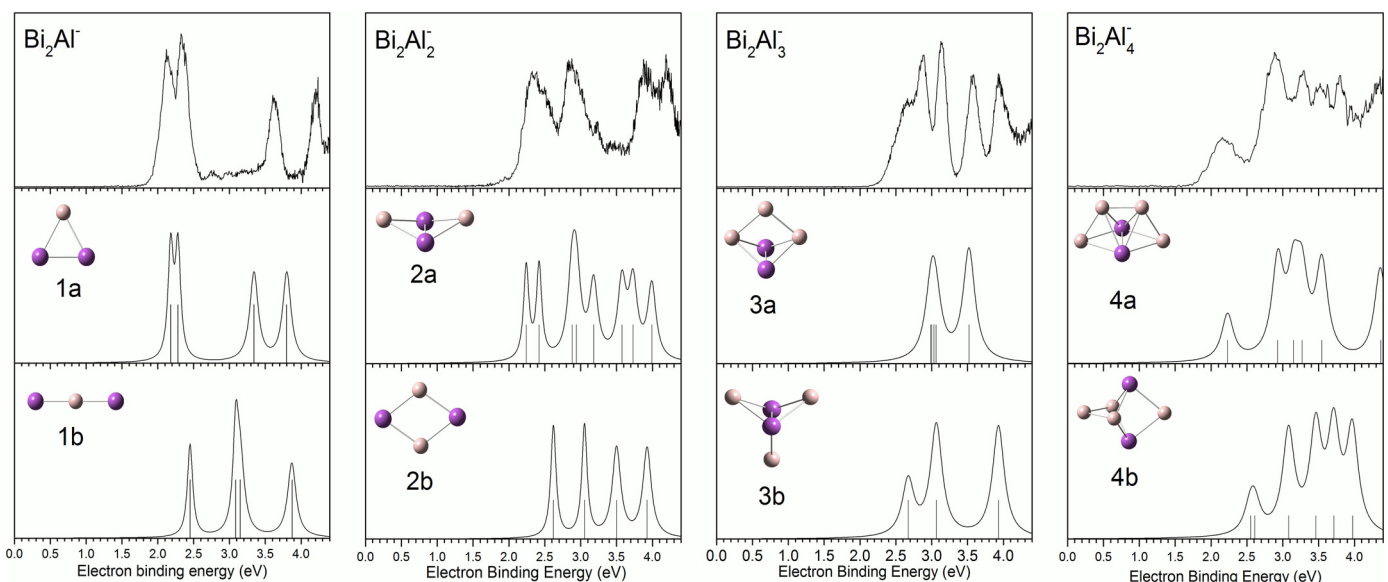


Figure 4. Comparison between the experimental photoelectron spectra and the simulated DOS spectra of the low-lying isomers of Bi_2Al_n^- ($n = 1\text{--}4$) cluster. The simulations were conducted by fitting the distribution of the transition lines with unit-area Lorentzian functions of 0.1 eV width.

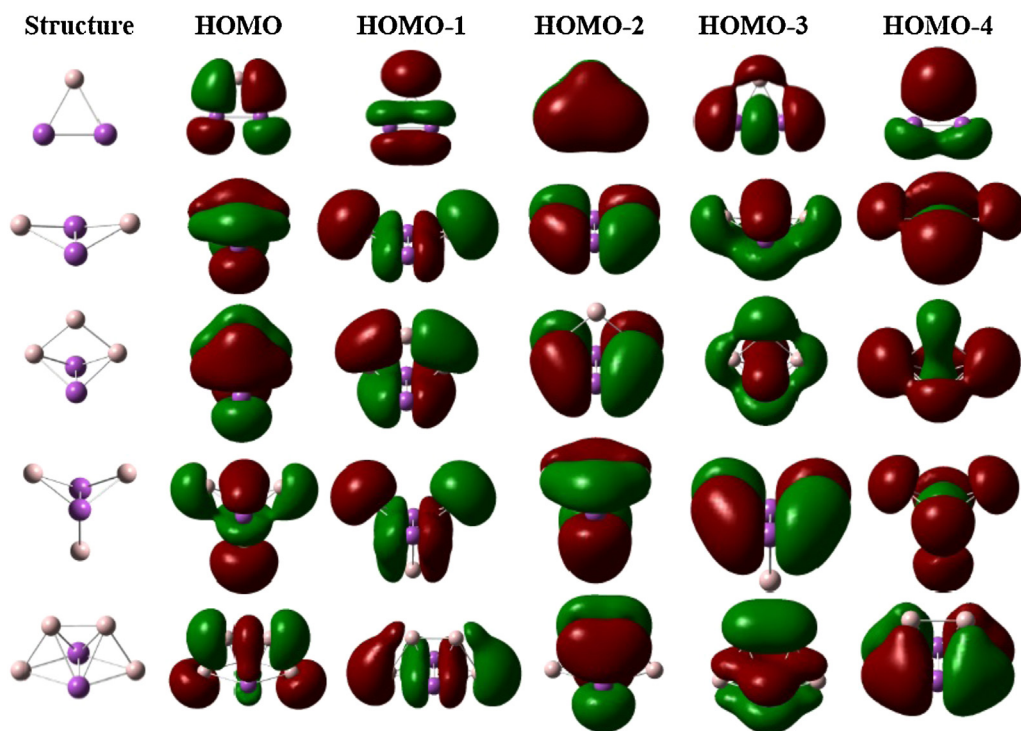


Figure 5. Molecular orbital pictures for the most possible structures of Bi_2Al_n^- ($n = 1\text{--}4$) cluster.

(2.15 eV), while the VDE of isomer 4b is 2.55 eV, much higher than the experimental result.

The comparison of the experimental PE spectrum of Bi_2Al_4^- with the simulated DOS spectra of isomers 4a and 4b is shown in Figure 4. The simulated DOS spectrum of isomer 4a is in agreement with the experimental PE spectrum, while the simulated spectrum of isomer 4b is not in agreement with the experimental one. Thus, we suggest that isomer 4a contributes to the measured PE spectrum of Bi_2Al_4^- anion.

From above analysis, we can see that the two Bi atoms tend to form Bi–Bi bond in the most stable structures of Bi_2Al_n^- ($n = 1\text{--}4$) clusters. The structures of Bi_2Al_n^- ($n = 1\text{--}4$) clusters are built from the Bi–Bi unit with increasing number of Al atoms. The geometric structures of Bi_2Al_n^- clusters transform from 2D to 3D configuration with increasing number of Al atoms.

It would be interesting to compare the structures of Bi_2Al_n^- ($n = 1\text{--}4$) clusters with their corresponding neutrals. The structures of neutral Bi_2Al and Bi_2Al_2 clusters are very similar to their corresponding anions except that the Bi–Al bonds are slightly longer and the Al–Al bonds are slightly shorter in the neutral clusters. For Bi_2Al_3 cluster, the structures of isomers 3A and 3B are similar to the most stable anionic structures (isomer 3a). Compared to isomer 3a, isomers 3A and 3B are distorted and have lower symmetries due to the removal of the excess electron. For neutral Bi_2Al_4 , the most stable structure is similar to the second stable structure of Bi_2Al_4^- anion. Therefore, the difference between anionic and neutral clusters of Bi_2Al_3 and Bi_2Al_4 indicates that the charge has effect on the stable geometric configuration for the big size clusters.

We conducted the natural population analysis to understand the electronic properties of anions and neutral of Bi_2Al_n ($n = 1\text{--}4$) clusters, and the charge distributions on Bi and Al atoms in the most probable isomers are presented in Tables 2 and 3 (the atom labels are displayed in the supporting information). As shown in Table 2, the negative charge on the two Bi atoms is higher than the sum of negative charge on the Al atoms, and the negative charges on the Bi_2 unit have little difference with the increase number of Al atoms. In addition, the natural populations of the two Bi atoms were found to

Table 2
NPA charge distributions in the most probable isomers of Bi_2Al_n^- ($n = 1\text{--}4$) clusters.

Cluster	Atom	NPA charge (e)	Cluster	Atom	NPA charge (e)
Bi_2Al^-	Bi1	-0.407	Bi_2Al_3^-	Bi1	-0.646
	Bi2	-0.407		Bi2	-0.646
	Al	-0.186		Al1	0.097
	Bi1	-0.532		Al2	0.097
	Bi2	-0.532		Al3	0.097
	Al1	0.032		Bi1	-0.398
Bi_2Al_2^-	Al2	0.032		Bi2	-0.398
	Bi1	-0.362		Al1	0.052
	Bi2	-0.362		Al2	0.052
	Al1	-0.030		Al3	-0.153
	Al2	-0.123		Al4	-0.153
	Al3	-0.123			
Bi_2Al_3^-	Bi1	-0.362			
	Bi2	-0.362			
	Al1	-0.030			
	Al2	-0.123			
	Al3	-0.123			
	Al4	-0.123			

Table 3
NPA charge distributions in the most stable structures of Bi_2Al_n ($n = 1\text{--}4$) clusters.

Cluster	Atom	NPA charge (e)	Cluster	Atom	NPA charge (e)
Bi_2Al	Bi1	-0.088	Bi_2Al_2	Bi1	-0.146
	Bi2	-0.088		Bi2	-0.146
	Al	0.176		Al1	0.146
				Al2	0.146
				Bi1	-0.433
				Bi2	-0.433
Bi_2Al_3	Bi1	-0.324	Bi_2Al_4	Al1	0.253
	Bi2	-0.073		Al2	0.093
	Al1	0.284		Al3	0.093
	Al2	0.153		Al4	0.426
	Al3	-0.040			

be negative in the neutral clusters from Table 3 because Bi element is more electronegative than Al element. Thus, this charge transfers from the Al atoms to the Bi_2 unit. Our results indicate that the Bi_2 unit in Bi_2Al_n^- ($n = 1\text{--}4$) clusters acts as an electron acceptor, influencing the electron populations and chemical bonding properties of the Al_n cluster framework.

5. Conclusions

The electronic and structural properties of Bi_2Al_n^- ($n=1-4$) cluster anions were studied by anion photoelectron spectroscopy and DFT calculations. The VDEs of Bi_2Al_n^- ($n=1-4$) clusters were estimated from their photoelectron spectra. The most probable structures of Bi_2Al_n^- ($n=1-4$) cluster anions were identified by comparing the calculated VDEs and the simulated DOS spectra to the experimental results. It is shown that the two Bi atoms tend to form Bi–Bi bond in the most stable structures of Bi_2Al_n^- ($n=1-4$) clusters. The NPA shows that the negative charges distribute mainly on the Bi–Bi unit in these clusters.

Acknowledgments

This work was supported by Scientific Research Fund of Hebei Provincial Department of Education (No. ZH2012023) and the Knowledge Innovation Program of the Chinese Academy of Sciences (Grant No. KJCX2-EW-H01). We are grateful to Prof. Zhen Gao for his advice on this letter.

Appendix A. Supplementary data

Supplementary data associated with this article can be found, in the online version, at doi:10.1016/j.cplett.2014.09.049.

References

- [1] I. Vurgaftman, J.R. Meyer, L.R. Ram-Mohan, *J. Appl. Phys.* 89 (2001) 5815.
- [2] R. Dai, S.G. Zhang, Y.B. Li, X. Guo, J.G. Li, *J. Alloys Compd.* 509 (2011) 2289.
- [3] W.R. Osório, E.S. Freitas, A. Garcia, *Electrochim. Acta* 108 (2013) 781.
- [4] H. Gomez, T.R. Taylor, D.M. Neumark, *J. Phys. Chem. A* 105 (2001) 6886.
- [5] H. Gomez, T.R. Taylor, Y. Zhao, D.M. Neumark, *J. Chem. Phys.* 117 (2002) 8644.
- [6] T.R. Taylor, H. Gomez, K.R. Asmis, D.M. Neumark, *J. Chem. Phys.* 115 (2001) 4620.
- [7] U. Gupta, J.U. Reveles, J.J. Melko, S.N. Khanna, A.W. Castleman Jr., *Chem. Phys. Lett.* 467 (2009) 223.
- [8] U. Gupta, J.U. Reveles, J.J. Melko, S.N. Khanna, A.W. Castleman Jr., *Chem. Phys. Lett.* 480 (2009) 189.
- [9] U. Gupta, J.U. Reveles, J.J. Melko, S.N. Khanna, A.W. Castleman Jr., *J. Phys. Chem. C* 114 (2010) 15963.
- [10] Z. Sun, Q. Zhu, Z. Gao, Z. Tang, *Rapid Commun. Mass Spectrom.* 23 (2009) 2663.
- [11] E.F. Archibong, D.S. Marynick, *Mol. Phys.* 101 (2003) 2785.
- [12] J.J. BelBruno, *Heteroatom Chem.* 14 (2003) 189.
- [13] L. Guo, H.-S. Wu, *Solid State Ionics* 177 (2006) 437.
- [14] L. Guo, *J. Mol. Struct.* 809 (2007) 181.
- [15] L. Guo, H.-S. Wu, *Eur. Phys. J. D* 42 (2007) 259.
- [16] C. Kamal, K.G. Tapan, B. Arup, C. Aparna, *J. Chem. Phys.* 130 (2009) 024308.
- [17] H.K. Quek, Y.P. Feng, C.K. Ong, *Z. Phys. D* 42 (1997) 309.
- [18] F. Li, L. Sun, J. Zhao, F. Xu, H.-Y. Zhou, Q.-M. Zhang, F.-L. Huang, *Int. J. Hydrogen Energy* 38 (2013) 6930.
- [19] C.E. Jones, P.A. Clayborne, J.U. Reveles, J.J. Melko, U. Gupta, S.N. Khanna, A.W. Castleman, *J. Phys. Chem. A* 112 (2008) 13316.
- [20] H.G. Xu, Z.G. Zhang, Y. Feng, J.Y. Yuan, Y.C. Zhao, W.J. Zheng, *Chem. Phys. Lett.* 487 (2010) 204.
- [21] A.D. Becke, *J. Chem. Phys.* 98 (1993) 5648.
- [22] C. Lee, W. Yang, R.G. Parr, *Phys. Rev. B* 37 (1988) 785.
- [23] C.E. Check, T.O. Faust, J.M. Bailey, B.J. Wright, T.M. Gilbert, L.S. Sunderlin, *J. Phys. Chem. A* 105 (2001) 8111.
- [24] W.R. Wadt, P.J. Hay, *J. Chem. Phys.* 82 (1985) 284.
- [25] E. van Lenthe, E.J. Baerends, J.G. Snijders, *J. Chem. Phys.* 99 (1993) 4597.
- [26] S. Sun, H. Liu, Z. Tang, *J. Phys. Chem. A* 110 (2006) 5004.
- [27] M.J. Frisch, et al., *Gaussian 03*, Gaussian Inc., Wallingford, CT, 2004.
- [28] J.P. Foster, F. Weinhold, *J. Am. Chem. Soc.* 102 (1980) 7211.
- [29] A.E. Reed, R.B. Weinstock, F. Weinhold, *J. Chem. Phys.* 83 (1985) 735.
- [30] A.E. Reed, L.A. Curtiss, F. Weinhold, *Chem. Rev.* 88 (1988) 899.
- [31] M.J. Frisch, et al., *Gaussian 09*, Gaussian Inc., Wallingford, CT, 2009.
- [32] M. Gausa, R. Kaschner, G. Seifert, J.H. Faehrmann, H.O. Lutz, K.H. Meiwes-Broer, *J. Chem. Phys.* 104 (1996) 9719.
- [33] M.A. Sobhy, J.U. Reveles, U. Gupta, S.N. Khanna, A.W. Castleman Jr., *J. Chem. Phys.* 130 (2009) 054304.
- [34] R. Kaschner, U. Saalmann, G. Seifert, M. Gausa, *Int. J. Quantum Chem.* 56 (1995) 771.
- [35] L. Gao, P. Li, H. Lu, S.F. Li, Z.X. Guo, *J. Chem. Phys.* 128 (2008) 194304.
- [36] D.J. Tozer, N.C. Handy, *J. Chem. Phys.* 108 (1998) 2545.
- [37] H. Hakkinen, B. Yoon, U. Landman, X. Li, H.J. Zhai, L.S. Wang, *J. Phys. Chem. A* 107 (2003) 6168.